Experimental demonstration of continuously variable optical encoding in a hybrid imaging system

Mads Demenikov, Gonzalo Muyo, and Andrew R. Harvey*

School of Engineering and Physical Sciences, Heriot Watt University, Edinburgh EH14 4AS, UK
Corresponding author: a.r.harvey@hw.ac.uk

We demonstrate an experimental method to obtain a continuously variable hybrid imaging system that uses two generalized cubic phase masks, to enable real-time optimization of the trade between extended depth-of-field and noise gain. We obtain point-spread functions as a function of the rotation angle and show an example of optimization based on recovered image quality.   © 2010 Optical Society of America

OCIS codes: 110.1758, 110.4850, 110.7348.

Hybrid imaging systems combine optical coding using pupil-plane phase modulation with postdetection image restoration to provide improved imaging performance or an additional degree of freedom in the system design process. Of particular interest is extension of the depth of field (DoF) and mitigation of optical aberrations [1–6]. Implementation of phase modulation involves a trade of improved DoF, determined by the amplitude of phase modulation, and noise amplification associated with suppression in the modulation-transfer function (MTF) [7]. We report here the first (to our knowledge) experimental demonstration of a simple technique employing rotating phase masks that enables continuously variable amplitude of phase modulation so that the optimum trade-off can be varied according to requirements. In comparison to the use of liquid-crystal modulation [8], this technique offers the advantage of high optical throughput and absence of polarization sensitivity.

Generation of various aberrations or phase modulations by lateral and longitudinal translation of two identical phase masks has been described by Palusinski *et al.* [9] and Mitchell and Sasian [10], respectively. Dowski [11] has shown that it is possible to continuously vary the net phase modulation and, hence, the DoF in a hybrid imaging system, by either rotation or lateral translation of two phase masks. We report here an experimental realization of an adjustable-DoF hybrid imaging system using two antisymmetric phase masks where one is rotated relative to the other. We describe first the principle of operation and then show experimental variation of point-spread functions (PSFs) and an experimental demonstration of optimization of amplitude of phase modulation. The form of each antisymmetric phase mask is described by a generalized cubic polynomial:

$$z(x,y) = \alpha(x^3 + y^3) + \beta(x^2 y + y^2 x), \qquad (1)$$

where x and y are normalized coordinates of the aperture stop and α and β define the phase modulation [4]. A phase mask with $\beta = -3\alpha$ has threefold rotational symmetry, as shown in Fig. 1(a), and can be employed to extend the DoF [4] or mitigate other defocus-related aberrations [6]. Rewriting Eq. (1) in polar form, with $\beta = -3\alpha$, $z(r,\theta) = \alpha r^3 \cos(3\theta)$, where r is normalized radius, enables the phase function applied by two phase masks with a relative rotation angle φ to be written as [11]

$$z(r,\theta,\varphi) = 2\cos(3\varphi/2)\alpha r^3 \cos(3\theta). \qquad (2)$$

Thus, the phase modulation retains a generalized cubic form with effective amplitude $\hat{\alpha} = 2\alpha\cos(3\varphi/2)$. This enables the degree of encoding to be continuously varied by simple rotation of one of the phase masks, as illustrated by the images of combined phase masks shown in Figs. 1(b) and 1(c). When $\varphi = 60°$, the modulations of the first mask are opposite to those of the second so that $\hat{\alpha} = 0$, whereas, for $\theta = 0°$, they sum as shown in Fig. 1(c) and $\hat{\alpha} = 2\alpha$.

We report here the experimental demonstration of this technique. Two phase masks were manufactured by laser polishing of fused silica plates with an active diameter of 12 mm and wavefront-modulation parameters $\alpha = 3.39\lambda$ and $\beta = -10.17\lambda$ ($\lambda = 550$ nm). These were mounted on rotation stages and located directly in front of a Nikon ED AF-S Nikkor 300 mm $f/4$D IF telephoto lens and aligned with its optical axis, as shown in Fig. 2. Images were recorded using a cooled Retiga 1300 camera (6.7 μm pixel pitch). Ideally, the phase masks should be located at the aperture stop of the lens to ensure that the phase modulation and, hence, the PSF, varies as little as possible across the field of view (FoV). In the experiments reported here, the FoV is relatively small and the modest variation of the PSF due to the suboptimal location of the phase plates is not a significant issue. The imaging performance in this demonstration is also slightly degraded by small high-order aberrations arising from the 10 mm spacing between the phase plates, but these aberrations could be avoided by mounting the plates in contact.

In the experimental setup, a spoke target is imaged in focus at a distance of 4 m from the lens and subsequently at a distance of 3.5 m, while the lens remained focused at 4 m. The measured in-focus PSF for $\varphi = 60°$
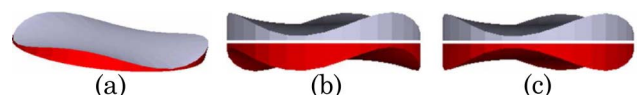

Fig. 1.   (Color online) Combination of two generalized cubic phase masks to control the amount of extended DoF: (a) single phase mask, where the values of α and β have been magnified (normally α and β are of the order of micrometers), (b) position of cancellation of extended DoF, and (c) maximum extended DoF.
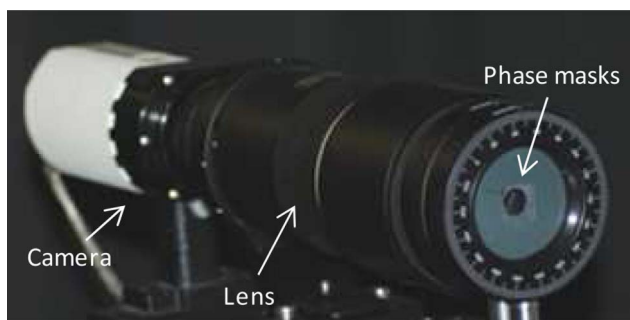
Fig. 2. (Color online) Experimental setup consisting of Nikon 300 mm lens, two generalized cubic phase masks on rotational stages, and a Retiga 1300 camera.

Fig. 4. Spoke target imaged with a phase mask rotated by (a), (e) 60°; (b), (f) 55°; (c), (g) 50°; and (d), (h) 45°. Upper row is in focus and lower row is defocused. All images have been restored using the optimum PSFs corresponding to the defocus distance. The optimal phase modulation is that given by 55° [(b), (f)], since this yields the highest contrast at both in- and out-of-focus. The variance is shown below each image.

(corresponding to $\alpha = 0$) is shown in Fig. 3(a), and Figs. 3(b)–3(d) show the PSFs for $\varphi = 55°$, $50°$, and $45°$; corresponding to $\hat{\alpha} = 0\lambda$, 0.88λ, 1.75λ, and 2.6λ. The PSFs show the expected variation from a near-diffraction-limited compact PSF for $\varphi = 60°$ to the characteristic extended PSF of a generalized cubic phase modulation as φ and, hence, $\hat{\alpha}$ are varied [4,6]. It is this extended PSF that enables imaging with increased DoF.

Images of the in-focus spoke target recorded with the phase plate oriented at the above angles and restored with a Wiener filter using the in-focus PSF as the kernel are shown in Figs. 4(a)–4(d). Images of the defocused spoke target recorded at the same orientations but restored using the defocused PSF as the kernel for the Wiener filter are shown in Figs. 4(e)–4(h). An objective in hybrid imaging is for the PSF to be invariant with respect to defocus, but, in practice, there are significant variations in the phase-transfer function such that artifacts are introduced when images are restored with a PSF corresponding to a different defocus [12]; here we use the ideal PSFs such that the recovered images correspond to the ideal artifact-free imaging performances.

It can be appreciated from the recovered images in Figs. 4(a)–4(d), and from the calculated image variances shown below each image, that, for in-focus imaging, there is a monotonic decrease in image contrast with increasing φ and $\hat{\alpha}$. This is due to the increased suppression of the MTF with increasing $\hat{\alpha}$. From Figs. 4(e)–4(h), it can be seen that, for the defocused images, the image contrast is lower for smaller and larger $\hat{\alpha}$ than for the intermediate value of $\hat{\alpha} = 0.88\lambda$ at $\varphi = 55°$. This is because, for small $\hat{\alpha}$, defocus introduces nulls in the MTF that cannot be restored by the Weiner filter, whereas, for large $\hat{\alpha}$, nulls are avoided, but excessive suppression of the MTF causes high levels of noise amplification by the Wiener filter. There is thus an optimum intermediate $\hat{\alpha}$ for a given
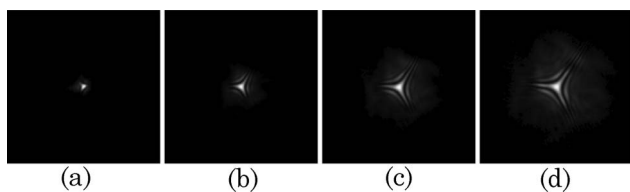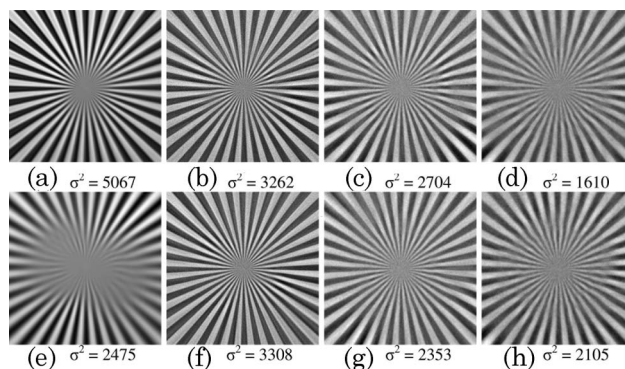

Fig. 3. Experimental PSFs as a function of relative angle between the two generalized phase masks: (a) 60°, (b) 55°, (c) 50°, (d) 45°.

defocus range that balances suppression of the MTF by defocus with that introduced by phase modulation [7]. In this case, $\hat{\alpha} = 0.88\lambda$ is close to optimal for mitigation of the given defocus of ± 500 mm, as can be appreciated by the higher level of image variance for Fig. 4(f). From a comparison of upper and lower images in Fig. 4, it can be seen that, for $\hat{\alpha} = 0$ ($\varphi = 60°$), the stated defocus has reduced image variance by about 50% and that degradation of image contrast is particularly severe at high frequencies, whereas, for higher values of $\hat{\alpha}$, image variance does not change appreciably with defocus and that good image contrast is retained for a wide range of frequencies. By comparison with the images for $\hat{\alpha} = 0$, however, the improved constancy of image quality with defocus for $\hat{\alpha} > 0$ is accompanied by a general reduction in signal-to-noise ratio (SNR).

In conclusion, we have described a relatively simple technique for implementing continuously variable amplitude of phase modulation and we have demonstrated this experimentally. While it is accepted that hybrid imaging offers scope for increased DoF, the SNR penalty is a major disincentive to its use, but we have conducted a laboratory demonstration of agile and experimental optimization of the trade of SNR for DoF. Extension to practical real-time imaging applications, providing a wide variation in DoF by employing a phase mask that rotates by as little as 5°, should be straightforward.

References

1. E. Dowski and T. W. Cathey, Appl. Opt. **34**, 1859 (1995).
2. W. Chi and N. George, Opt. Lett. **26**, 875 (2001).
3. S. Mezouari, G. Muyo, and A. R. Harvey, J. Opt. Soc. Am. A **23**, 1058 (2006).
4. S. Prasad, V. P. Pauca, R. J. Plemmons, T. C. Torgersen, and J. van der Gracht, Proc. SPIE **5559**, 335 (2004).
5. M. Demenikov, E. Findlay, and A. R. Harvey, Opt. Express **17**, 6118 (2009).
6. G. Muyo, A. Singh, M. Andersson, D. Huckridge, A. Wood, and A. R. Harvey, Opt. Express **17**, 21118 (2009).
7. T. Vettenburg, N. Bustin, and A. R. Harvey, Opt. Express **18**, 9220 (2010).

8. G. Carles, G. Muyo, S. Bosch, and A. R. Harvey, J. Mod. Opt. (2010).
9. I. A. Palusinski, J. M. Sasian, and J. E. Greivenkamp, Appl. Opt. **38**, 86 (1999).
10. T. A. Mitchell and J. M. Sasian, Proc. SPIE **3705**, 209 (1999).
11. E. Dowski, "Mechanically-adjustable optical phase filters for modifying depth of field, aberration-tolerance, anti-aliasing in optical systems," U.S. patent 7,180,673 (February 20, 2007).
12. M. Demenikov and A. R. Harvey, Opt. Express **18**, 8207 (2010).